ACCOUNTS
of chemical research

Solution and Solid State NMR Approaches To Draw Iron Pathways in the Ferritin Nanocage

DANIELA LALLI AND PAOLA TURANO*

CERM and Department of Chemistry, University of Florence, via Sacconi 6, 50019, Sesto Fiorentino, Florence, Italy

RECEIVED ON APRIL 8, 2013

CONSPECTUS

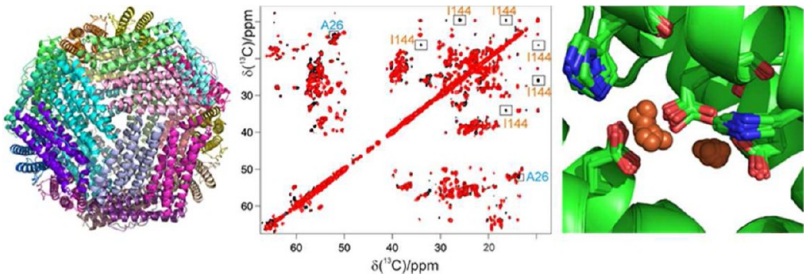

Ferritins are intracellular proteins that can store thousands of iron(III) ions as a solid mineral. These structures autoassemble from four-helix bundle subunits to form a hollow sphere and are a prototypical example of protein nanocages. The protein acts as a reservoir, encapsulating iron as ferric oxide in its central cavity in a nontoxic and bioavailable form. Scientists have long known the structural details of the protein shell, owing to very high resolution X-ray structures of the apoform. However, the atomic level mechanism governing the multistep biomineralization process remained largely elusive.

Through analysis of the chemical behavior of ferritin mutants, chemists have found the role of some residues in key reaction steps. Using Mössbauer and XAS, they have identified some di-iron intermediates of the catalytic reaction trapped by rapid freeze quench. However, structural information about the iron interaction sites remains scarce. The entire process is governed by a number of specific, but weak, interactions between the protein shell and the iron species moving across the cage. While this situation may constitute a major problem for crystallography, NMR spectroscopy represents an optimal tool to detect and characterize transient species involving soluble proteins.

Regardless, NMR analysis of the 480 kDa ferritin represents a real challenge. Our interest in ferritin chemistry inspired us to use an original combination of solution and solid state approaches. While the highly symmetric structure of the homo-24-mer frog ferritin greatly simplifies the spectra, the large protein size hinders the efficient coherence transfer in solution, thus preventing the sequence specific assignments. In contrast, extensive ^{13}C-spin diffusion makes the solution ^{13}C$-^{13}$C NOESY experiment our gold standard to monitor protein side chains both in the apoprotein alone and in its interaction with paramagnetic iron species, inducing line broadening on the resonances of nearby residues. We could retrieve the structural information embedded in the ^{13}C$-^{13}$C NOESY due to a partial sequence specific assignment of protein backbone and side chains we obtained from solid state MAS NMR of ferritin microcrystals. We used the 59 assigned amino acids (~33% of the total) as probes to locate paramagnetic ferric species in the protein cage. Through this approach, we could identify ferric dimers at the ferroxidase site and on their pathway towards the nanocage. Comparison with existing data on bacterioferritins and bacterial ferritins, as well as with eukaryotic ferritins loaded with various nonfunctional divalent ions, allowed us to reinterpret the available information.

The resulting picture of the ferroxidase site is slightly different with various ferritins but is designed to provide multiple and generally weak iron ligands. The latter assist binding of two incoming iron(II) ions in two proximal positions to facilitate coupling with oxygen. Subsequent oxidation is accompanied by a decrease in the metal−metal distance (consistent with XAS/Mössbauer) and in the number of protein residues involved in metal coordination, facilitating the release of products as di-iron clusters under the effect of new incoming iron(II) ions.

Structure of Protein Nanocages

Protein nanocages self-assemble from multiple subunits giving rise to highly symmetrical polyhedral hollow architectures (Figure 1), a feature shared by several systems which also have in common the ability to sequester their cargo within the cage. X-ray crystallography and, in larger

Published on the Web 09/03/2013 www.pubs.acs.org/accounts
10.1021/ar4000983

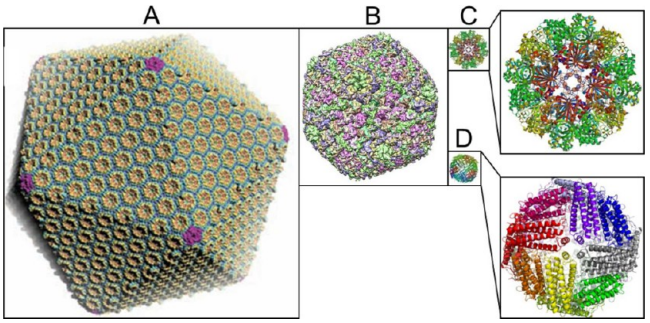

FIGURE 1. Some protein nanocages: (A) carboxysome;[2] (B) human adenovirus capsid (PDB id 1VSZ); (C) SOR (PDB id 2YAV); (D) maxiferritin (PDB id 3RBC).

structures, a combination of X-ray and cryo-EM provided the structural description of these complex molecular assemblies.

In icosahedral or quasi-spherical viruses (Figure 1B), the protein coat forming the capsid is composed of multiple copies of one protein or several copies of few different proteins, arranged in hexagonal structures to form 20 triangular faces. At each of the 12 vertices of the icosahedral architecture (with diameters ranging from 18 to 500 nm),[1] five subunits make contact symmetrically. The viral capsid embeds the nucleic acid of the virus.

Analogously, bacterial microcompartments are formed by thousands of copies of a limited number of proteins arranged in an icosahedral structure with 100−200 nm diameter, generally resulting from a combination of hexameric and pentameric units. Similar to virus capsids, the pentamers generate curvature and occupy the 12 vertices (Figure 1A).[2] The shell proteins surround a lumen containing tens to hundreds of copies of a few specific enzymes that constitute a short metabolic pathway. The cavity is used to enhance reactivity by elevating the levels of the substrates in close proximity of the embedded enzymes. Substrates and products diffuse in and out from the cavity.

In other nanocages, the enzymatic activity derives directly from the proteins that form the cage shell. An example is the sulfur oxygenase reductase (SOR, Figure 1C), the initial enzyme of the sulfur oxidation pathway in some thermoacidophilic Archaea, as well as mesophilic and thermophilic bacteria. The essentially spherical hollow architecture is composed of 24 identical subunits.[3] Chimney-like structures protruding from the external surface at the 4-fold symmetry axes and with hydrophobic internal walls have been proposed to modulate the access of the sulfur to the inner cavity. The oxygen-dependent sulfur disproportionation reaction occurs at a mononuclear non-heme iron center in the protein shell that can be accessed by sulfur from the inner cavity through a narrow pore. Product exit might occur via hydrophilic channels with outlets at the 3-fold symmetry axes.

A 24-mer hollow sphere architecture also characterizes bacterioferritin and maxiferritins (Figure 1D).[4,5] These proteins have a smooth external surface and four-helix bundle subunits. The curvature of the bundle axis essentially defines the curvature of the protein shell surface. Helices H1−H2 and H3−H4 within each subunit form antiparallel pairs, with H1 and H3 at the external surface and H2 and H4 providing the cage wall. An external long loop extends along the helix-bundle and connects H2 and H3 (Figure 2). A short fifth helix (H5) is angled about 60° from the bundle axis (Figure 2E). The resulting architecture has an outer diameter of about 12 nm and an internal cage diameter on the order of 8 nm (Figure 2A,B). Extended intersubunit contacts involving helices H1 and H2 as well as the long loop give rise to dimers interacting along C2 symmetry axes (Figure 2A). The surface is pierced by pores at the 3-fold (C3) and 4-fold (C4) symmetry axes where three and four subunits come in contact (Figure 2C,D). Main differences between maxiferritins from different organisms and between ferritins and bacterioferritins are the length and shape of loops connecting the four helices. In bacterioferritins, intersubunit contacts are characterized by the presence of b-type hemes at the dimer interfaces.[6] In mammals, the ferritin multimers are hetero-oligomers resulting from the combination of two types of subunits in variable proportion (L and H chains) that differ in sequence up to 35−40%.

The complex ferritin architecture is designed to let iron(II) enter the protein and reach the catalytic site (ferroxidase or oxidoreductase site) where the two substrates, iron(II) and O_2, couple to provide di-iron(III) mineral precursors that then evolve to form a concentrated ferric biomineral core stored within the protein shell.[4]

Dodecameric bacterial ferritin homologues (miniferritins or DPSs, DNA-binding protein from starved cells) share a similar four-helix bundle structure, but the extra short helix is located between the second and third helices in the monomer bundle.[4] The central cavity has a diameter on the order of 4−5 nm, while the outer diameter is about 9 nm. As a consequence, in DPS proteins only up to 500 iron(III) ions can be stored, which compares with a total capacity of about 4500 ferric ions for maxiferritins.

In bacterioferritins and in prokaryotic maxiferritins, a di-iron binding center (identified as the ferroxidase site) is present about halfway from the N- and C-termini of the helix bundle, as revealed by X-ray crystallography.[7−9] When we

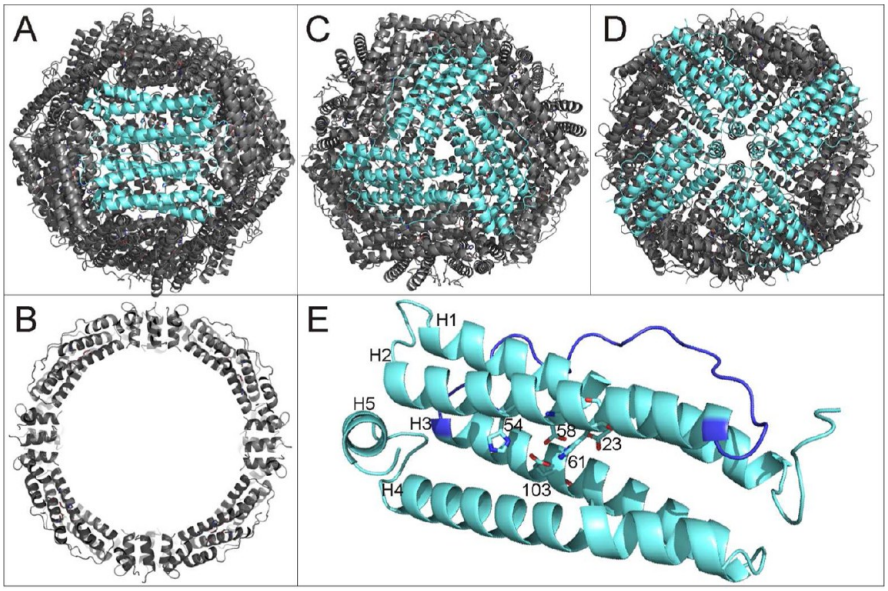

FIGURE 2. Different views of frog M ferritin (PDB id 1MFR) highlighting in cyan the symmetry-related subunits: (A) C2 axis with extended intersubunit helical contacts governing the self-assembly process; (B) the large inner cavity; channels at the (C) C3 axis and (D) C4 axis; (E) the four-helix bundle (helices H1−H4) subunit, and short helix H5 and iron ligands (sticks) at the ferroxidase site.

entered the field, the only available structure of an iron-bound eukaryotic ferritin was of marine pennate diatoms *Pseudo-nitzschia multiseries*,[10] which is largely divergent from other eukaryotic ferritins. No iron-bound crystal structure was available for ferritins from higher eukaryotes, but only structures with divalent cations as redox-stable alternative for iron(II), namely, zinc(II) in human H ferritin and magnesium(II) in frog ferritin (a homopolymer formed by M subunits similar to mammalian H chains).[11,12] These structures showed a dimetal center in the internal central positions of the four-helix bundle with different number and nature of the metal ligands with respect to the ferroxidase sites in bacterial ferritins and bacterioferritins and in the catalytic sites of di-iron enzymes.[7,8,13,14] The difficulty in detecting iron at the ferroxidase site in eukaryotic ferritins has been ascribed to the transient nature of this site where, at variance with metalloenzymes, iron is not the catalytic center, but is a substrate that has to be released to migrate toward the nanocavity to form the biomineral. In bacterioferritins, the iron is generally stably bound at a symmetric dinuclear site with terminal glutamate/histidine ligands and two bridging glutamates.[8] In *Pseudomonas aeruginosa* bacterioferritin, iron at a similar site could be trapped only upon flash-freezing of Fe-soaked crystals.[9]

Why NMR?

Ferritin-mediated biomineralization is a multistep reaction dominated by iron trafficking processes. The ferrous ions enter the protein shell, most probably through the C3 pores[15,16] and diffuse to the ferroxidase site, in the middle of the four-helix bundle. Based on Mössbauer and XAS measurements at low temperature,[17] upon reaction, an initial diferrous, high-spin state forms with an Fe−Fe distance of 3.44 Å. After 25 ms, a peroxodiferric intermediate, with the very short Fe−Fe distance of 2.53 Å, appears and rapidly (about 1 min) evolves toward a diferric μ-oxo/hydroxo species with a Fe−Fe distance of 3.00 Å. It was commonly accepted that, upon formation, the diferric μ-oxo/hydroxo species should translocate from the catalytic to the biomineralization site. From the biomineral, iron is then released in response to signals of iron requirement. The entire process requires a number of weak transient interactions between the protein matrix and the ferrous and ferric species. NMR represents a key investigation tool to reveal transient interactions between protein amino acids and other chemical entities including metal ions[18] and internal protein dynamics on various time scales.[19]

Paramagnetic iron species can be located via the NMR-detectable hyperfine unpaired electron(s)−nuclear coupling. The hyperfine interactions manifest themselves through an extra contribution to the nuclear chemical shift and a reduction of the nuclear relaxation times and consequent NMR-signal broadening. Of the three main sources of paramagnetic contributions to nuclear relaxation (contact, dipolar, and Curie-spin), the Curie-spin interaction, which depends upon r^{-6}, with r being the nucleus−paramagnetic

center distance, is largely dominant for high molecular weight systems at high magnetic fields.[20] These conditions apply to ferritin studied at magnetic fields ≥700 MHz.

Feasibility of Solution NMR Experiments for a 480 kDa Protein Nanocage

Two main problems characterize the NMR spectra of high molecular weight proteins: spectral crowding and signal broadening. Chemical shifts of the NMR active nuclei typically used to record spectra of proteins (i.e., ^{1}H, ^{15}N, and ^{13}C) span a limited range of values; increasing molecular size in general implies an increased number of signals in the same chemical shift interval, severely compromising spectral resolution. Protein nanocages constitute a particularly favorable example of high molecular weight assemblies because they are composed of several repeats of a few different protein subunits in symmetric architectures. Corresponding nuclei in symmetry-related protein chains experience the same chemical environment and therefore exhibit the same chemical shift. This is the case of frog ferritin, a symmetric homopolymer of 24 identical M subunits, each composed of 175 amino acids. All the experiments reported in this Account refer to this sample system, where the spectral complexity is expected to be significantly reduced, with a total number of signals equal to that provided by a single subunit.

The feasibility of NMR spectroscopy in large supramolecular assemblies is limited by signal line width, which is the result of the fast nuclear transverse relaxation for large molecules in solution and may become so severe that signals in ^{1}H NMR experiments are severely broadened, as in the case of the ferritin 24-mer (480 kDa). Main contributions to transverse relaxation are the slow molecular tumbling in solution and the ^{1}H−^{1}H dipolar couplings. Reducing the tumbling time is difficult because it would require low viscosity solvents or high temperatures, two experimental conditions that are difficult to achieve when dealing with biological macromolecules. The rotation correlation time, τ_r, of frog ferritin at 298 K measured by nuclear magnetic relaxation dispersions (NMRD)[21] is about 130 ns. It decreases down to about 50 ns only when temperature is increased to 338 K, far too high to ensure protein stability in long-lasting high-resolution NMR experiments. Line-narrowing in ^{1}H NMR spectra can be achieved by replacement of nonexchangeable protons by deuterons, thus reducing ^{1}H−^{1}H dipolar couplings.[22] Up to 90% deuteration of ferritin was not sufficient to enable the efficient use of solution NMR experiments based on ^{1}H-detection (Figure 3A). The slow molecular tumbling of ferritin broadens beyond detection

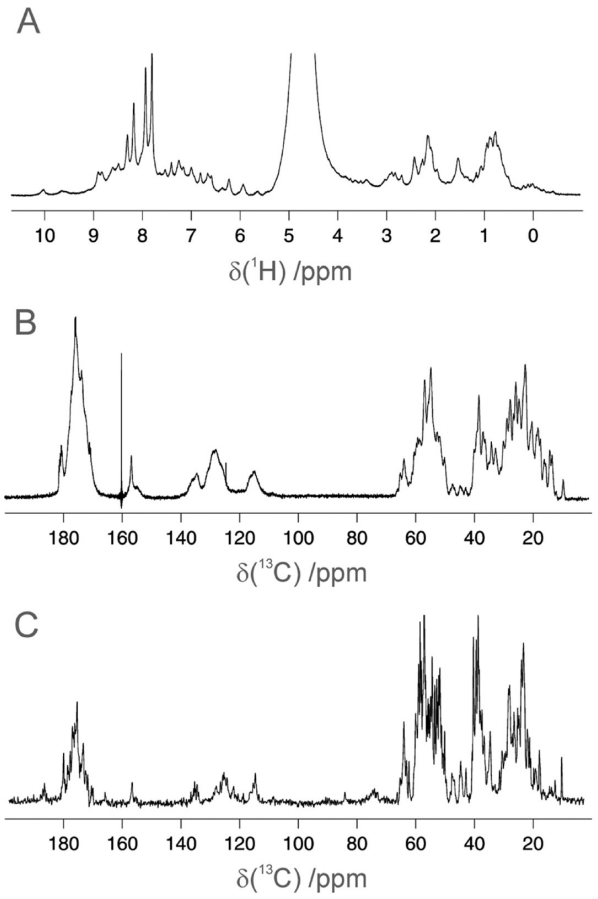

FIGURE 3. Monodimensional NMR spectra of frog ferritin at 298 K: (A) solution ^{1}H at 900 MHz; (B) solution ^{13}C at 900 MHz; (C) solid state ^{13}C at 700 MHz and 9 kHz MAS rate. Sample enrichment: solution, ^{2}H, ^{13}C, ^{15}N; solid state, ^{13}C, ^{15}N.

essentially all signals in standard ^{1}H−^{15}N HSQC experiments (Figure 4A) and in their TROSY (transverse relaxation-optimized spectroscopy) version (Figure 4B). Even cross-correlated relaxation-enhanced polarization transfer (CRINEPT)-TROSY experiments (Figure 4C), which have been successfully applied to observe the signals of low-to-medium size proteins in complexes of total molecular weight from 100 kDa[23] to 1 MDa,[24] permit the observation only of a subset of the expected signals.

We therefore abandoned ^{1}H-detection in favor of ^{13}C-detection. Nuclear relaxation rates are proportional to the square of the gyromagnetic ratios of the nuclei giving rise to the various relaxation mechanisms. As a consequence of the smaller gyromagnetic ratio of ^{13}C compared with ^{1}H (6.73×10^{7} vs 2.67×10^{8} rad T^{-1} s^{-1}), ^{13}C-detected NMR has been useful for studying systems where ^{1}H NMR finds limitations due to fast nuclear relaxation.[25,26] This is the case of ferritin, where monodimensional ^{13}C spectra show a sensibly higher resolution than the corresponding monodimensional ^{1}H

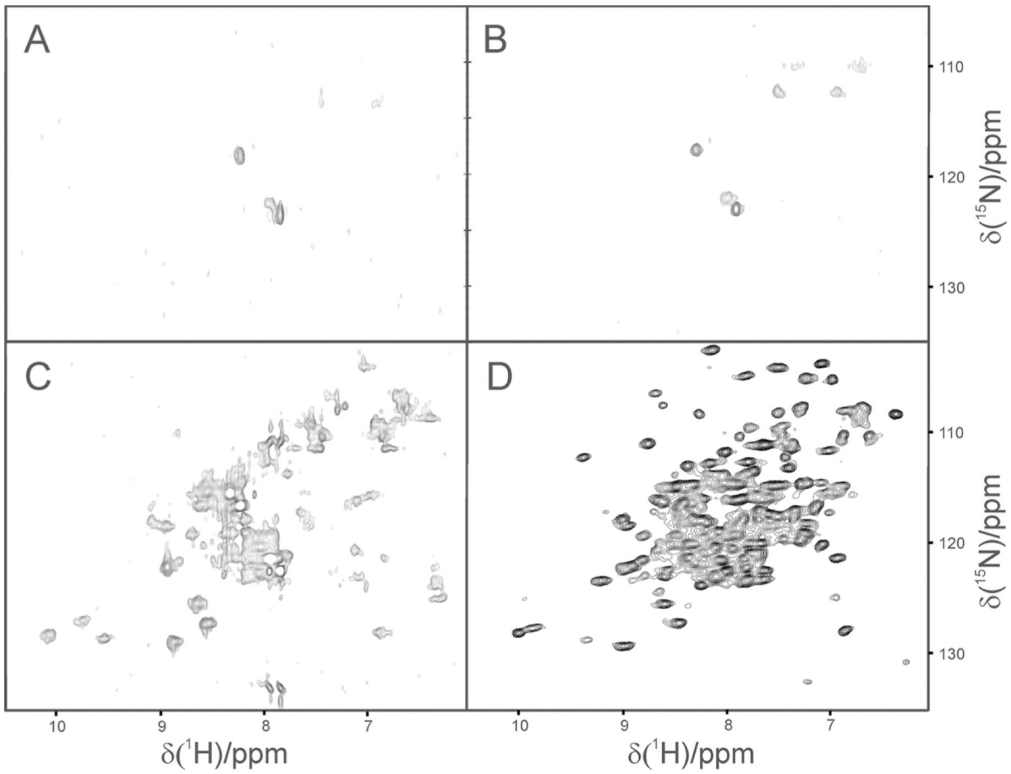

FIGURE 4. $^{1}H-^{15}N$ correlation experiments on $^{2}H,^{15}N$ frog ferritin in solution (900 MHz, 298 K): (A) HSQC; (B) TROSY; (C) (CRINEPT)-TROSY. (D) SS $^{1}H-^{15}N$ correlation spectrum ($^{2}H,^{13}C,^{15}N$ ferritin with 30% back-exchanged amide protons, 850 MHz, 1.3 mm probe, 60 kHz MAS rate, approximately 298 K).

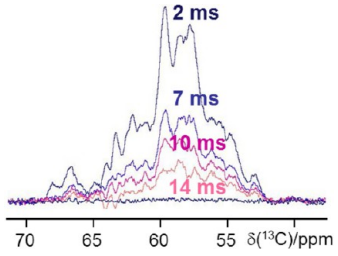

FIGURE 5. $^{13}C\alpha$ signal loss as a function of the spin-lock time used to keep magnetization transverse.[27]

spectra (Figure 3B): ^{13}C transverse relaxation properties of aliphatic signals in perdeuterated samples allow observation of resonances with linewidths on the order of 50–100 Hz and thus can be exploited in high-resolution studies.

Nevertheless, significant loss of coherence occurs when ^{13}C magnetization is transverse, as shown by ^{13}C 1D spin–echo experiments on the Cα region (Figure 5).[27] Transverse relaxation during the delays needed to build heteronuclear coherence is so severe that it has prevented successful acquisition of any of the experiments for sequence-specific assignments using protonless-NMR pulse sequences.

In contrast, $^{13}C-^{13}C$ NOESY experiments of ferritin proved extremely useful. Magnetization transfer phenomena, the basis of NOESY experiments, occur when the magnetization is along the *z*-axis and are determined by two main processes: cross relaxation, responsible for the magnetization transfer through dipolar coupling, and longitudinal relaxation, which restores the magnetization to equilibrium values. The longitudinal relaxation times are substantially long in large proteins; the cross-relaxation in homonuclear experiments increases with the rotation correlation time of the molecule and therefore with molecular weight.[28] Therefore, efficient spin diffusion through networks of directly bound ^{13}C spins is established, giving rise to sensitive $^{13}C-^{13}C$ NOESY spectra for ferritin (Figure 6A).[29] With appropriate mixing times, the NOESY maps of ferritin contain complete correlations between networks of carbon spins belonging to the same amino acid[29] and were used to identify spin systems arising from specific amino acid types, a kind of information that is generally available from $^{1}H-^{1}H$ TOCSY spectra of small soluble proteins. By taking advantage of the residue-specific chemical shifts of carbon nuclei, we identified the spin patterns of about 75% of the total amino acids using intraresidue NOESY connectivities.

The shortest inter-residue C–C distances in proteins are those between carbonyls and between carbonyls and Cα of sequential amino acids (2.4–2.9 Å). Due to resolution

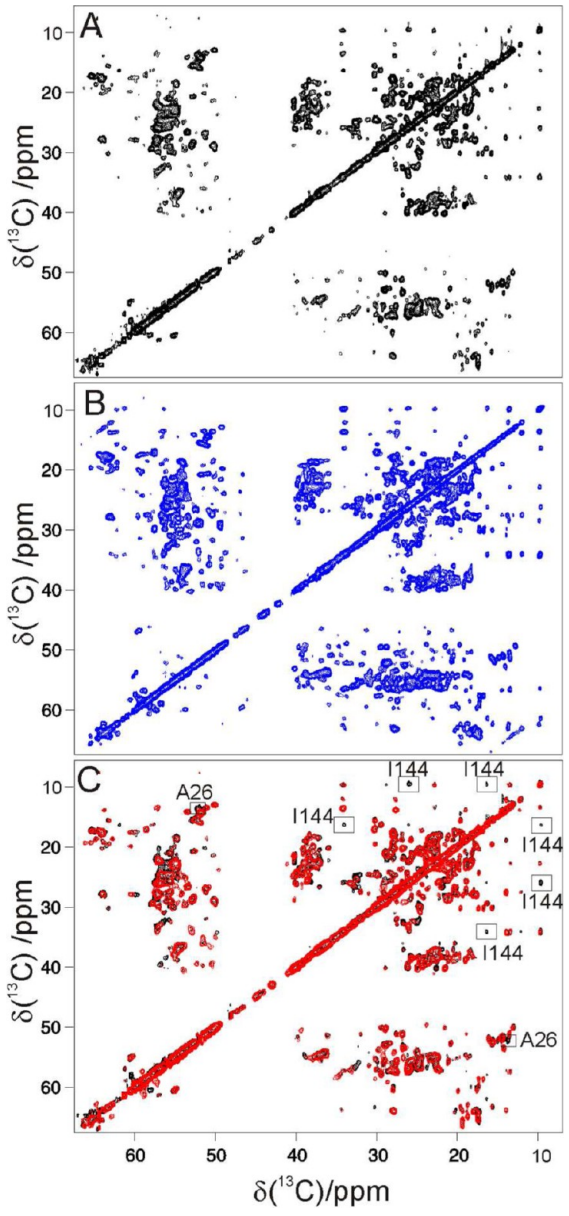

FIGURE 6. Aliphatic region of (A) solution $^{13}C-^{13}C$ NOESY of $^{2}H,^{13}C,^{15}N$ ferritin at 700 MHz, 298 K, 500 ms mixing time and (B) SS $^{13}C-^{13}C$ DARR of $^{13}C,^{15}N$ ferritin at 700 MHz, 298 K, 9 kHz MAS rate, 40 ms mixing time. (C) Superimposition of solution $^{13}C-^{13}C$ NOESY spectra (aliphatic region; spectral acquisition parameters as in panel A) of apo-ferritin (black trace) and ferritin loaded with two iron(II) ions/subunit (red trace).

problems, mainly arising from the extremely broad carbonyl resonances, we could analyze neither CO−CO nor CO−Cα peaks. In the X-ray crystal structure of ferritin, all the other inter-residue connectivities involving pairs of carbon atoms fall at distances larger than 3.2 Å and could not be observed. Therefore, no inter-residue information could be derived from $^{13}C-^{13}C$ NOESY.

In summary, while NOESY was selected as our gold standard to monitor conformational changes and interactions of ferritin in solution, the problem of achieving a sequential assignment remained unsolved.

Solid State NMR as a Tool for Sequential Assignment

Immobilization of proteins in the solid state overcomes the problems arising from the rapid transverse relaxation due to slow tumbling in solution making magic angle spinning (MAS) solid state (SS) NMR suitable for protein analysis. However, for moderate MAS rates, it is difficult to remove the ^{1}H dipolar couplings even in SS and the resulting ^{1}H linewidths are prohibitive for constructive use.[30] Therefore, SS NMR studies of biomolecules are traditionally performed by directly detecting ^{13}C via ^{1}H-enhanced cross-polarization. SS NMR of ferritin microcrystals provided relatively well-resolved monodimensional ^{13}C spectra (Figure 3C). The $^{13}C-^{13}C$ correlation SS experiments (proton-driven spin diffusion (PDSD) or dipolar-assisted rotational resonance (DARR)) and the $^{13}C-^{13}C$ solution NOESY (Figure 6A,B) are essentially superimposable and provide the same information about spin patterns because they all rely on spin diffusion effects along amino acid side chains. High similarity between solution and SS spectra implies that the protein does not undergo major conformational changes attributable to crystal packing effects upon formation of microcrystals and guarantees a straightforward transfer of the assignments to the solution state.

Assignment of SS spectra was based on three commonly used heteronuclear experiments:[31] NCACX that gives intraresidue $N_i-C\alpha_i-CX_i$ connectivities; NCOCX and CANCO that provide sequential connectivities of the type $N_i-CO_{i-1}-CX_{i-1}$ and $C\alpha_i-N_i-CX_{i-1}$, respectively. In particular, a 3D NCACX spectrum was used to confirm the C−C intraresidue connectivities observed in solution $^{13}C-^{13}C$ NOESY and to identify the intraresidue backbone amide nitrogen. Then, sequential assignments were obtained by matching ^{15}N shifts in the NCACX and NCOCX spectra and from CANCO experiments that provide direct connectivities between backbone atoms of adjacent amino acids. Several factors complicated spectral analysis: (i) the intrinsically low chemical shift dispersion due to the four-helix bundle structure of the subunits; (ii) the primary sequence of ferritin, with large numbers (36%) of residues with narrow and overlapping distribution of ^{13}C chemical shifts (19 leucine and 13 lysine, 18 glutamate and 13 aspartate), and (iii) the difficulty in discriminating among glutamate, glutamine, aspartate, and asparagine. Nevertheless, 59 residues were sequence-specifically assigned, distributed on helices H1, H3, H4, and

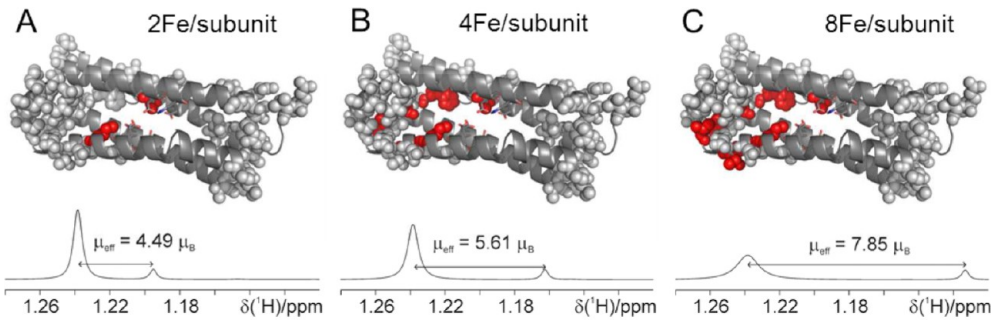

FIGURE 7. Assigned resonances (gray spheres) that become broadened beyond detection (red spheres) upon addition of (A) two iron(II)/subunit; (B) four iron(II)/subunit, and (C) eight iron(II)/subunit. Chemical shift differences used to derive bulk magnetic susceptibility and resulting magnetic moments are reported in the lower panels.

H5 (Figure 7).[32] Their chemical shift index is consistent with their location on the expected secondary structure elements, and DARR spectra on a sample expressed in [2-^{13}C]-labeled glycerol[33] confirmed the chemical nature of the observed residues.

Iron Oxidation Products: Paramagnetic NMR and Complementary X-ray Crystallography

The solution $^{13}C-^{13}C$ NOESY represented our spectroscopic tool to monitor the reaction with iron following the behavior of the assigned residues.

As reported,[17] the first step of iron biomineralization is the oxidation at the ferroxidase active site of two ferrous ions to a diferric oxo/hydroxo species. We therefore titrated a solution of $^{2}H,^{13}C,^{15}N$-enriched ferritin by additions of two iron(II) ions per subunit until eight iron atoms/subunit were reached and acquired a $^{13}C-^{13}C$ NOESY map after each addition.[32]

The Ferroxidase Site. The first two iron(II) ions react with oxygen and are immediately converted into iron(III) species, as shown by changes in absorption spectra. Some signals of apoferritin resonating in well-resolved spectral regions of the $^{13}C-^{13}C$ NOESY and well outside the noise level (Figure 6C) were broadened beyond detection, possibly due to the paramagnetism of the iron(III) products on resonances of nearby residues. We verified this hypothesis by measuring the bulk magnetic susceptibility in solution at different steps of the iron titration (Figure 7). The species formed from the first two iron(II) ions/subunit has μ_{eff} of 4.5μ_B, consistent with an antiferromagnetically coupled μ-oxo ferric dimer such as observed by Mössbauer.[17] In a 480 kDa protein, paramagnetic transverse relaxation is dominated by the Curie relaxation:[20] any nucleus within 5 Å from either of the two ferric ions is expected to be broadened beyond detection. Luckily, resolved resonances broadened beyond detection belong to assigned residues

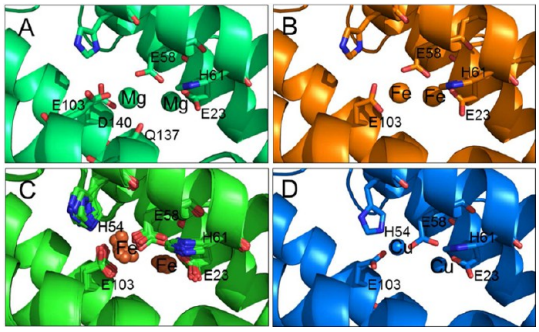

FIGURE 8. Coordination environment of different metal ions at the ferroxidase site: (A) magnesium(II) (PDB id 1MFR); (B) iron(III) (90 min-soaking; PDB id 3RBC); (C) iron(II)/iron(III) (1 min-soaking) in the 24 independent subunits (PDB id 3RGD); (D) copper(II) (PDB id 3RE7).

(Ile144 and Ala26). Significantly, the resonances of Ile141 were not affected. When we published these data,[32] the only available structure for frog ferritin containing a metal ion was that with magnesium(II) (Figure 8A).[11] The observed paramagnetic broadening could not be reconciled with the position of magnesium(II), which is closer to Ile141 than to Ile144. Upon assuming that the structure of the magnesium adduct is a good model for the iron(II) binding site, we concluded that, upon formation, iron(III) products have to leave the binding site of the divalent metal ions.

This initial proposal was revised by us later on, when we solved the X-ray crystal structure of iron-loaded ferritin,[16] the only example of a higher eukaryotic ferritin with iron at the ferroxidase site. This achievement was possible by flash freezing crystals soaked for different times in iron(II) solutions under aerobic conditions: for 90 min soaking (Figure 8B), all 24 independent subunits present in the crystal asymmetric unit contain a single iron dimer, with Fe–Fe average distance of 3.1 Å, strongly supportive of the presence of a μ-oxo/hydroxo bridge iron. As expected for a species that should only transiently interact at this site, the Fe–Fe moiety is loosely anchored to the protein, with one

iron ion (Fe1) bound to Glu23, bridging Glu58 and His61, and the other (Fe2) binding to the bridging Glu58 and bidentate Glu103. For short soaking times (1 min), the 24 independent subunits show different ferric dimers at the ferroxidase site (Figure 8C): while the situation at the Fe1 site corresponds to that observed for 90 min-soaking, at the Fe2 site two different clusters of iron ions are observed, one essentially overlapping with that of Figure 8B and the other at a longer distance from Fe1 and forming a coordination bond with His54 that assumes a different conformation. This second cluster closely resembles the structure of copper(II) bound to ferritin (Figure 8D),[16] and we have attributed it to iron trapped in the initial docking site of the ferrous state.

Afterward, in a paper reporting iron binding experiments via ITC, EPR and Mössbauer in *Pyrococcus furiosus* and human H ferritin, Hagen and co-workers reproposed the same type of interpretation of our paramagnetic-broadening NMR data that we had reached based on our crystallographic data, that is, (i) the iron(III) and iron(II) binding sites are essentially coincident but differ in the nature of ligands with respect to that of magnesium(II) and (ii) the iron site remains occupied during reaction turnovers.[34] Hagen also proposed as a general mechanism of ferritin that incoming iron(II) displaces only one of the two iron(III) ions of the diferric center leading to the formation of a mixed valence Fe(II)−Fe(III) species and displacement of a single iron(III) ion that moves to form the biomineralization core. This picture was supported by the presence of a third iron ion close to the active site in *P. furiosus* structure that has never been observed in iron-loaded M ferritin crystals. In *Pseudomonas aeruginosa* bacterioferrin, a gated access to the site via one of the iron-ligand histidines has been suggested.[9]

In our view, the general applicability of a common model for ferritin mechanism has still to be proven. We are therefore focusing our discussion on M ferritin as our reference system. A few considerations emerge from our data and comparison with recent literature on this protein: (i) copper(II), cobalt(II), and iron(II) bind at a site that differs from that of magnesium(II) for some ligands; (ii) two iron(II) ions bind at the ferroxidase site in a coordination environment that involves His54; (iii) oxidation and formation of diferric oxo/hydroxo bridges stabilize the cluster, imposing a shorter intermetal distance and destabilizing the binding to the protein (detachment of His54); (iv) the iron binding site identified by crystallography is fully consistent with paramagnetic broadening effects observed in $^{13}C-^{13}C$ NOESY in solution.

Paramagnetic broadening in NMR spectra persists days after addition of iron(II); therefore the ferroxidase site remains occupied for long times. This observation has to be reconciled with the fact that X-ray crystallography is able to detect iron dimers only in samples flash-frozen in liquid N_2. Probably ferric dimers may occupy multiple close positions at this loosely coordinating ferroxidase site, which may interconvert. NMR reports only average effects and settles the ferric products in the surroundings of Ile144 and Ala26. X-ray detects iron only when these fluxional situations are frozen into a major conformer. Uptake of iron(II) substrate and release of iron(III) products at the catalytic site requires a number of weak binding ligands that accompany these dynamic processes with local conformational changes. X-ray data on different metal ions or on ferritins with different sequence report slightly different situations. Given the high number of amino acid side chains in the ferritin shell that may act as metal ligands, crystal soaking in iron or cocrystallization with different metals lead to the observation of ions at nonfunctional positions. NMR has proven useful to select those sites that better reflect the solution state.

Formation of Biomineral Precursors. Subsequent additions of iron(II) in steps of two ions/subunit translated into an increased number of resonances broadened beyond detection (Figure 7). Interestingly, the iron(III) site always remains populated as proven by the fact that the signals of Ile144 and Ala26 are always affected by paramagnetic broadening. The species responsible for the more extended paramagnetic broadening observed with four iron ions/subunit has a total effective magnetic moment of $5.6\mu_B$, that is, sensibly lower than expected for two independent iron(III)-dimers of the type observed at the first addition, suggesting the presence of a magnetically coupled four-iron(III) cluster.

With a stoichiometry of eight iron ions/subunit, the paramagnetic effects extend from the ferroxidase site up to 20 Å from it, toward helix H5. The total effective magnetic moment of $7.8\mu_B$ compares well with that measured for some $Fe_8(\mu_4\text{-}O)_4$ model systems,[35] while the magnetic moment per ion is further reduced, suggesting the formation of clusters of higher nuclearity. Upon addition of eight iron ions/subunit or more, paramagnetic broadening involves residues located close to the N-terminal end of the bundle, probably because, within antiparallel subunit dimers at the C2 axes, the C-terminal end of one subunit gets close to the N-terminal end of the adjacent subunit and intersubunit paramagnetic effects become visible, complicating the analysis.

These broadening effects led to the suggestive hypothesis that biomineral precursors form inside the channel and merge at the C4 axes,[32] which is something that still needs to be proven by higher resolution methods.

The mechanism emerging from NMR is that new incoming iron(II) ions substitute the di-iron(III) moiety and get oxidized; the new diferric species has some magnetic coupling with previously formed products; the ferroxidase center is always occupied, but the nascent polynuclear clusters settle in a protein area that extends from the ferroxidase center to the H5 helix.

Ongoing Research and Outlook

For its size, ferritin represents a challenge for NMR; interest in ferritin chemistry has inspired the development of innovative NMR approaches. Partial spectral assignment has provided information about the ferroxidase site and the fate of the ferric products. While the former has been better identified by crystallography, the latter escaped detection via X-ray. A more extended assignment would help to define iron−protein interactions at higher resolution via NMR. Ultrafast MAS SS NMR made it possible to obtain $^{1}H-^{15}N$ HSQC of much better quality than the corresponding solution spectra (Figure 4D), because under these spinning rates the ^{1}H dipolar couplings are heavily weakened,[36] and the resolution introduced by the ^{1}H-dimension should permit extension of the sequence specific assignment. Finally, the recently proposed metal-mediated assembly/disassembly of ferritin, which provides stable subunits in pure form and intact structure,[37] opens new routes:[38] assignment of a single monomer is indeed affordable with standard solution NMR approaches.

Ferritin can be considered a prototype of protein nanocages. Application of our combined solution−solid state approach and of technical advances under development on M ferritin to other homopolymeric ferritins and bacterioferritins is expected to be straightforward. In heteropolymeric ferritins or nanocages composed by different proteins, selective labeling of a single type of protein chain per time should provide spectra of reasonable quality, because the number of amino acids per chain is never so high to induce unacceptable crowding of signals. Breaking of the molecular symmetry due to uneven distribution of the different types of subunits, instead, is expected to be deleterious in terms of spectral complexity. The upper limit of molecular weight for the feasibility of solution $^{13}C-^{13}C$ NOESY experiments is still unknown; while the efficiency of NOE transfer is expected to increase with increasing molecular dimensions, detection of NMR signals above a certain size threshold may become unfeasible.

The sedimented solute NMR (SedNMR),[39] developed on ferritin, might be further exploited to study iron−ferritin interactions for its ability to detect weak interactions in large adducts.[40]

While stable functional complexes involving nanocages[41] are better suited for X-ray characterization, SedNMR might be applied to weak adducts between nanocages and small proteins.[40] However, $^{13}C-^{13}C$-correlated maps are not particularly suitable to this purpose due to the poor sensitivity of ^{13}C chemical shift to changes in the chemical environment of the nucleus; the applicability of SedNMR for the detection of $^{1}H-^{15}N$ correlated spectra of large supramolecular assemblies is not yet demonstrated.

Our warmest thanks to the late Ivano Bertini for inspiration and support. We are indebted to Elizabeth Theil for initiating us into the ferritin world and proficuous collaboration. We acknowledge Stefano Mangani for X-ray crystallography, and Ente Cassa di Risparmio di Firenze and MIUR-PRIN2009 for financial support.

BIOGRAPHICAL INFORMATION

Daniela Lalli studied Chemistry at the University of Florence (M.Sc. in Chemistry of Biological Molecules in 2007; Ph.D. in Chemical Sciences in 2011). She is currently a postdoctoral fellow with Paola Turano.

Paola Turano is Associate Professor of General and Inorganic Chemistry at the University of Florence since 2002. Her main research activities include development and application of solution and solid state NMR approaches to proteins and their complexes.

FOOTNOTES

*Corresponding author. Telephone: +39-0554574266. Fax: +39-0554574253. E-mail: turano@cerm.unifi.it.

The authors declare no competing financial interest.

REFERENCES

1 Douglas, T.; Young, M. Viruses: Making Friends with Old Foes. *Science* **2006**, *312*, 873–875.

2 Tanaka, S.; Kerfeld, C. A.; Sawaya, M. R.; Cai, F.; Heinhorst, S.; Cannon, G. C.; Yeates, T. O. Atomic-Level Models of the Bacterial Carboxysome Shell. *Science* **2008**, *319*, 1083–1086.

3 Urich, T.; Gomes, C. M.; Kletzin, A.; Frazão, C. X-ray Structure of a Self-Compartmentalizing Sulfur Cycle Metalloenzyme. *Science* **2006**, *311*, 996–1000.

4 Liu, X.; Theil, E. C. Ferritins: Dynamic Management of Biological Iron and Oxygen Chemistry. *Acc. Chem. Res.* **2005**, *38*, 167–175.

5 Crichton, R. R.; Declercq, J. P. X-ray Structures of Ferritins and Related Proteins. *Biochim. Biophys. Acta* **2010**, *1800*, 706–718.

6 Yasmin, S.; Andrews, S. C.; Moore, G. R.; Le Brun, N. E. A New Role for Heme, Facilitating Release of Iron from the Bacterioferritin Iron Biomineral. *J. Biol. Chem.* **2011**, *286*, 3473–3483.

7 Tatur, J.; Hagen, W. R.; Matias, P. M. Crystal Structure of the Ferritin from the Hyperthermophilic Archaeal Anaerobe Pyrococcus furiosus. *J. Biol. Inorg. Chem.* **2007**, *12*, 615–630.

8 Crow, A.; Lawson, T. L.; Lewin, A.; Moore, G. R.; Le Brun, N. E. Structural Basis for Iron Mineralization by Bacterioferritin. *J. Am. Chem. Soc.* **2009**, *131*, 6808–6813.

9 Weeratunga, S. K.; Lovell, S.; Yao, H.; Battaille, K. P.; Fischer, C. J.; Casey, E. G.; Rivera, M. Structural Studies of Bacterioferritin B (BfrB) from Pseudomonas aeruginosa Suggest a Gating Mechanism for Iron Uptake via the Ferroxidase Center. *Biochemistry* **2010**, *49*, 1160–1175.

10 Marchetti, A.; Parker, M. S.; Moccia, L. P.; Lin, E. O.; Arrieta, A. L.; Ribalet, F.; Murphy, M. E.; Maldonado, M. T.; Armbrust, E. V. Ferritin Is Used for Iron Storage in Bloom-Forming Marine Pennate Diatoms. *Nature* **2009**, *457*, 467–470.

11 Ha, Y.; Shi, D.; Small, G. W.; Theil, E. C.; Allewell, N. M. Crystal Structure of Bullfrog M Ferritin at 2.8 Å Resolution: Analysis of Subunit Interactions and the Binuclear Metal Center. *J. Biol. Inorg. Chem.* **1999**, *4*, 243–256.

12 Toussaint, L.; Bertrand, L.; Hue, L.; Crichton, R. R.; Declercq, J. P. High-Resolution X-ray Structures of Human Apoferritin H-Chain Mutants Correlated with Their Activity and Metal-Binding Sites. *J. Mol. Biol.* **2007**, *365*, 440–452.

13 Schwartz, J. K.; Liu, X. S.; Tosha, T.; Theil, E. C.; Solomon, E. I. Spectroscopic Definition of the Ferroxidase Site in M Ferritin: Comparison of Binuclear Substrate Vs Cofactor Active Sites. *J. Am. Chem. Soc.* **2008**, *130*, 9441–9450.

14 Tosha, T.; Hasan, M. R.; Theil, E. C. The Ferritin Fe2 Site at the Diiron Catalytic Center Controls the Reaction with O2 in the Rapid Mineralization Pathway. *Proc. Natl. Acad. Sci. U. S. A* **2008**, *105*, 18182–18187.

15 Tosha, T.; Ng, H.-L.; Bhattasali, O.; Alber, T.; Theil, E. C. Moving Metal Ions through Ferritin-Protein Nanocages from Three-Fold Pores to Catalytic Sites. *J. Am. Chem. Soc.* **2010**, *132*, 14562–14569.

16 Bertini, I.; Lalli, D.; Mangani, S.; Pozzi, C.; Rosa, C.; Theil, E. C.; Turano, P. Structural Insights into the Ferroxidase Site of Ferritins from Higher Eukaryotes. *J. Am. Chem. Soc.* **2012**, *134*, 6169–6176.

17 Hwang, J.; Krebs, C.; Huynh, B. H.; Edmondson, D. E.; Theil, E. C.; Penner-Hahn, J. E. A Short Fe-Fe Distance in Peroxodiferric Ferritin: Control of Fe Substrate versus Cofactor Decay? *Science* **2000**, *287*, 122–125.

18 Crowley, P. B.; Ubbink, M. Close Encounters of the Transient Kind: Protein Interactions in the Photosynthetic Redox Chain Investigated by NMR Spectroscopy. *Acc. Chem. Res.* **2003**, *36*, 723–730.

19 Fragai, M.; Luchinat, C.; Parigi, G. "Four-Dimensional" Protein Structures: Examples from Metalloproteins. *Acc. Chem. Res.* **2006**, *39*, 909–917.

20 Bertini, I.; Turano, P.; Vila, A. J. Nuclear Magnetic Resonance of Paramagnetic Metalloproteins. *Chem. Rev.* **1993**, *93*, 2833–2932.

21 Fabry, M. E.; Koenig, S. H.; Schillinger, W. E. Nuclear Magnetic Relaxation Dispersion in Protein Solutions. *J. Biol. Chem.* **1970**, *245*, 4256–4262.

22 Sattler, M.; Fesik, S. W. Use of Deuterium Labeling in NMR: Overcoming a Sizeable Problem. *Structure* **1996**, *4*, 1245–1249.

23 Caillet-Saguy, C.; Piccioli, M.; Turano, P.; Izadi-Pruneyre, N.; Delepierre, M.; Bertini, I.; Lecroisey, A. Mapping the Interaction between the Hemophore HasA and its Outer Membrane Receptor HasR using CRINEPT-TROSY NMR Spectroscopy. *J. Am. Chem. Soc.* **2009**, *131*, 1736–1744.

24 Riek, R.; Wider, G.; Pervushin, K.; Wüthrich, K. Polarization Transfer by Cross-Correlated Relaxation in Solution NMR with Very Large Molecules. *Proc. Natl. Acad. Sci. U.S.A.* **1999**, *96*, 4918–4923.

25 Oh, B.-H.; Westler, W. M.; Darba, P.; Markley, J. L. Protein Carbon-13 Spin Systems by a Single Two-Dimensional Nuclear Magnetic Resonance Experiment. *Science* **1988**, *240*, 908–911.

26 Bermel, W.; Bertini, I.; Felli, I. C.; Piccioli, M.; Pierattelli, R. ^{13}C-Detected Protonless NMR Spectroscopy of Proteins in Solution. *Prog. NMR Spectrosc.* **2006**, *48*, 25–45.

27 Bermel, W.; Bertini, I.; Felli, I. C.; Matzapetakis, M.; Pierattelli, R.; Theil, E. C.; Turano, P. A Method for C^{α} Direct-Detection in Protonless NMR. *J. Magn. Reson.* **2007**, *188*, 301–310.

28 Bertini, I.; Felli, I. C.; Kümmerle, R.; Luchinat, C.; Pierattelli, R. ^{13}C-^{13}C NOESY: A Constructive Use of ^{13}C-^{13}C Spin-Diffusion. *J. Biomol. NMR* **2004**, *30*, 245–251.

29 Matzapetakis, M.; Turano, P.; Theil, E. C.; Bertini, I. ^{13}C-^{13}C NOESY Spectra of a 480 kDa Protein: Solution NMR of Ferritin. *J. Biomol. NMR* **2007**, *38*, 237–242.

30 Thompson, L. K. Solid-State NMR Studies of the Structure and Mechanisms of Proteins. *Curr. Opin. Struct. Biol.* **2002**, *12*, 661–669.

31 Li, Y.; Berthold, D. A.; Frericks, H. L.; Gennis, R. B.; Rienstra, C. M. Partial C-13 and N-15 Chemical-Shift Assignments of the Disulfide-Bond-Forming Enzyme DsbB by 3D Magic-Angle Spinning NMR Spectroscopy. *ChemBioChem* **2007**, *8*, 434–442.

32 Turano, P.; Lalli, D.; Felli, I. C.; Theil, E. C.; Bertini, I. NMR Reveals a Pathway for Iron Mineral Precursors to the Central Cavity of Ferritin. *Proc. Natl. Acad. Sci. U.S.A.* **2010**, *107*, 545–550.

33 Castellani, F.; van Rossum, B.; Diehl, A.; Schubert, M.; Rehbein, K.; Oschkinat, H. Structure of a Protein Determined by Solid-State Magic-Angle-Spinning NMR Spectroscopy. *Nature* **2002**, *420*, 98–102.

34 Honarmand Ebrahimi, K.; Bill, E.; Hagedoorn, P. L.; Hagen, W. R. The Catalytic Center of Ferritin Regulates Iron Storage via Fe(II)-Fe(III) Displacement. *Nat. Chem. Biol.* **2012**, *8*, 941–948.

35 Baran, P.; Boca, R.; Chakraborty, I.; Giapintzakis, J.; Herchel, R.; Huang, Q.; McGrady, J. E.; Raptis, R. G.; Sanakis, Y.; Simopoulos, A. Synthesis, Characterization, and Study of Octanuclear Iron-Oxo Clusters Containing a Redox-Active Fe_4O_4-Cubane Core. *Inorg. Chem.* **2008**, *47*, 645–655.

36 Knight, M. J.; Webber, A. L.; Pell, A. J.; Guerry, P.; Barbet-Massin, E.; Bertini, I.; Felli, I. C.; Gonnelli, L.; Pierattelli, R.; Emsley, L.; Lesage, A.; Hermann, T.; Pintacuda, G. Fast Resonance Assignment and Fold Determination of Human Superoxide Dismutase by High-Resolution Proton-Detected Solid State MAS NMR Spectroscopy. *Angew. Chem., Int. Ed.* **2011**, *50*, 11697–11701.

37 Huard, D. J.; Kane, K. M.; Tezcan, F. A. Re-engineering Protein Interfaces Yields Copper-Inducible Ferritin Cage Assembly. *Nat. Chem. Biol.* **2013**, *9*, 169–176.

38 Theil, E. C.; Turano, P. Metalloenzymes: Cage Redesign Explains Assembly. *Nat. Chem. Biol.* **2013**, *9*, 143–144.

39 Bertini, I.; Luchinat, C.; Parigi, G.; Ravera, E.; Reif, B.; Turano, P. Solid-State NMR of Proteins Sedimented by Ultracentrifugation. *Proc. Natl. Acad. Sci. U.S.A.* **2011**, *108*, 10396–10399.

40 Bertini, I.; Luchinat, C.; Parigi, G.; Ravera, E. SedNMR: on the edge between solution and solid state NMR. *Acc. Chem. Res.* **2013**, DOI: 10.1021/ar300342f.

41 Yao, H.; Wang, Y.; Lovell, S.; Kumar, R.; Ruvinsky, A. M.; Battaille, K. P.; Vakser, I. A.; Rivera, M. The Structure of the BfrB-Bfd Complex Reveals Protein-Protein Interactions Enabling Iron Release from Bacterioferritin. *J. Am. Chem. Soc.* **2012**, *134*, 13470–13481.